Supporting Information for

Impacts of tile drainage on hydrology, soil biogeochemistry, and crop yield in the U.S. Midwestern agroecosystems

Zewei Ma[1,2,3], Kaiyu Guan[1,2,3,4*], Bin Peng[1,2,5*], Wang Zhou[1,2,6], Robert Grant[7], Jinyun Tang[8], Murugesu Sivapalan[9,10], Ming Pan[11], Li Li[12], Zhenong Jin[13]

[1]Agroecosystem Sustainability Center, Institute for Sustainability, Energy, and Environment, University of Illinois Urbana-Champaign, Urbana, IL 61801, USA.

[2]Department of Natural Resources and Environmental Sciences, College of Agricultural, Consumer and Environmental Sciences, University of Illinois Urbana-Champaign, Urbana, IL 61801, USA

[3]DOE Center for Advanced Bioenergy and Bioproducts Innovation, Urbana, IL, United States

[4]National Center for Supercomputing Applications, University of Illinois Urbana-Champaign, Urbana, IL 61801, USA

[5]Department of Crop Sciences, College of Agricultural, Consumer and Environmental Sciences, University of Illinois Urbana-Champaign, IL, 61801, USA

[6]School of Agriculture, Shenzhen Campus of Sun Yat-sen University, Shenzhen, China

[7]Department of Renewable Resources University of Alberta, Alberta, T6G2E3, Canada

[8]Climate Sciences Department, Lawrence Berkeley National Laboratory, CA, 94720, USA

[9]Department of Civil and Environmental Engineering, University of Illinois Urbana-Champaign, Urbana, IL 61801, USA

[10]Department of Geography and Geographic Information Science, University of Illinois Urbana-Champaign, Urbana, IL 61801, USA

[11]Scripps Institution of Oceanography, University of California San Diego, La Jolla, CA 92037, USA

[12]Department of Civil and Environmental Engineering, The Pennsylvania State University, University Park, PA 16802, USA

[13]Department of Bioproducts and Biosystems Engineering, University of Minnesota-Twin Cities, Saint Paul, MN 55108, USA

Corresponding author: Kaiyu Guan (kaiyug@illinois.edu), Bin Peng (binpeng@illinois.edu)

Contents of this file

Supplemented text

Text S1. Surface water flux

Surface water balance is achieved by considering precipitation (including irrigation), evaporation, lateral water fluxes, and infiltration,

$$\frac{\partial(dA)}{\partial t} + \frac{\partial q_x}{\partial x} + \frac{\partial q_y}{\partial y} = P - i - E \quad (S1)$$

where d is the surface water depth $[m]$; A is the area of the grid $[m^2]$; q_x and q_y is the surface water fluxes in x and y direction, respectively $[m^3\ h^{-1}]$. P is the precipitation, including irrigation $[m^3\ h^{-1}]$; i is the soil infiltration $[m^3\ h^{-1}]$; E is the evaporation from bare soil and litter on the soil surface $[m^3\ h^{-1}]$. The surface water fluxes are estimated using kinematic wave theory with Manning's equation:

$$q_x = \frac{d^{\frac{5}{3}} S_x^{0.5}}{n} \quad (S2)$$

$$q_x = \frac{d^{\frac{5}{3}} S_y^{0.5}}{n} \quad (S3)$$

where S_x and S_y are the slope gradient components along the x and y directions, respectively $[m\ m^{-1}]$; n is Manning's roughness coefficient $[m^{-1/3}\ h]$. Soil evaporation is estimated with soil and litter vapor density and boundary layer resistance,

$$E = E_{soil} + E_{litter} \quad (S4)$$

$$E_{soil} = \frac{e_{air} - e_{soil}}{r_s} A \quad (S5)$$

$$E_{litter} = \frac{e_{air} - e_{litter}}{r_l} A \quad (S6)$$

where E_{soil} and E_{litter} are the soil evaporation and litter evaporation $[m^3\ h^{-1}]$, respectively; e_{air}, e_{soil}, and e_{litter} are the vapor density in air, soil, and litter $[m^3\ m^{-3}]$, respectively. r_s and r_l are the soil and litter boundary resistance $[h\ m^{-1}]$.

Text S2. Subsurface water fluxes

The soil water flow in *ecosys* is governed by Richards' equation,

$$\frac{\partial \theta_w}{\partial t} = \frac{\partial}{\partial z}\left(K(\theta_w)\left(\frac{\partial h}{\partial z} + 1\right)\right) - S \quad (S7)$$

where θ_w is the soil water content $[m^3\ m^{-3}]$; $K(\theta_w)$ is the soil hydraulic conductance at θ_w $[m/h]$. S is soil water sink term $[m^3\ m^{-3}\ h^{-1}]$, including plant and mycorrhizal water uptake, lateral water fluxes to the external water table, and discharge to tile pipes.

Water fluxes to (from) the external water table and tile pipes are simulated with Darcy's flow in saturated soil,

$$v = \frac{K\Delta D}{d} \quad (S8)$$

where v is the flow velocity $[m/h]$; K is the saturated hydraulic conductance $[m/h]$; ΔD is the pressure drop $[m]$ over a distance d $[m]$. In the calculation of the lateral water flux to the external water table, the pressure drop is defined as the difference between internal water table depth and external water table depth $(D_3 - D_1)$, and the distance is then defined as the distance to the external water table (d_1). A positive velocity indicates water leaving the field to the external water table, and a negative velocity indicates water entering the field from the external water table. For the tile flow, the pressure drop is defined as the difference between internal water table depth and tile depth $(D_2 - D_1)$, and the distance is then defined as half of the tile space (d_2). Tile flow only occurs in soil layers above the tile pipes. There is no tile flow if

the water table in the field is below the tile pipes. The water table in the field is in the lowest unsaturated soil layer below which all soil layers are saturated. Specifically, the water table in the field is estimated with,

$$D_1 = \left(d_s - \frac{L_i \theta_i}{\theta_{i,s}} \right) \quad (S9)$$

where D_1 is the water table depth $[m]$, d_s is the depth to the top of the uppermost saturated soil layer $[m]$, L_i is the thickness of the lowest unsaturated soil layer $[m]$, θ_i is the volumetric soil water content of the lowest unsaturated soil layer $[m^3/m^3]$, $\theta_{i,s}$ is the saturated volumetric soil water content of the lowest unsaturated soil layer $[m^3/m^3]$.

Text S3. Soil solute and gas transport

All the gases and solutes (i.e., O_2, H_2, N_2, NH_3, CH_4, N_2O, CO_2, NO_2^-, NO_3^-, NH_4^+, and PO_4^{3-}) undergo convective-dispersive transfer among soil layers and through roots in each soil layer driven by concentration gradients and dispersivities.

$$Q_g = -Q_w C_g + D_g \frac{\partial C_g}{\partial L} \quad (S10)$$

$$Q_s = Q_w C_s + D_s \frac{\partial C_s}{\partial L} \quad (S11)$$

$$D_g = \frac{D_g' f_{t,g} {\theta_g}^2}{\theta_p^{0.67}} \quad (S12)$$

$$D_s = D_q |Q_w| + D_s' f_{t,s} \theta_w \tau \quad (S13)$$

where Q_g is the gaseous flux of a certain gas in soil $[g\ m^{-2}\ h]$; Q_w is the water flow rate in the soil $[m^3\ m^{-2}\ h^{-1}]$. C_g is the gaseous concentration of certain gas in soil $[g\ m^{-3}]$; D_g is the gaseous diffusivity of a certain gas in soil $[m^2 h^{-1}]$, determined by gaseous diffusivity at 0 °C (D_g') $[m^2 h^{-1}]$, temperature dependence function for gaseous diffusivity ($f_{t,g}$) [-], the air-filled porosity (θ_g) $[m^3\ m^{-3}]$, and soil porosity (θ_p) $[m^3 m^{-3}]$; $\frac{\partial C_g}{\partial L}$ is the concentration gradient of a certain gas in soil $[g\ m^{-3} m^{-1}]$; Q_s is the solute flux of a certain solution in soil $[g\ m^{-2}\ h]$; C_s is the solute concentration of the solution in soil $[g\ m^{-3}]$; D_s is the solute diffusivity of the solution in soil $[m^2 h^{-1}]$, determined by dispersivity in soil (D_q) $[m]$, the solute diffusivity at 0 °C (D_s') $[g\ m^{-2}\ h]$, Q_w, temperature dependence function for solute diffusivity ($f_{t,s}$) [-], the soil water filled porosity (θ_w) $[m^3\ m^{-3}]$; τ is the soil tortuosity [-].

All gases undergo volatilization – dissolution between the gaseous and solute phases in the soil and root.

$$Q_{d,\lambda} = a_g D_{d,\lambda} \left(S_\lambda' f_{t,s,\lambda} \left(C_{g,\lambda} - C_{s,\lambda} \right) \right) \quad (S14)$$

where $Q_{d,\lambda}$ is volatilization – dissolution of a certain gas (λ) between solute and gaseous phases $[g\ m^{-2}\ h]$; a_g is the air-water interfacial area $[m^2 m^{-2}]$; S_λ' is the Ostwald solubility coefficient of a certain gas at 30 °C [-]; $f_{t,s,\lambda}$ is the temperature dependence function of S_λ' [-]; $C_{g,\lambda}$ is the gaseous concentration of certain gas in soil $[g\ m^{-3}]$; $C_{s,\lambda}$ is the corresponding solute concentration in soil $[g\ m^{-3}]$.

Gases exchange also happens between the atmosphere and the soil surface, determined by the gas concentration in the soil and atmosphere, boundary layer conductance, and gaseous diffusivity:

$$Q_{g,\lambda,surface} = g_a \left\{ C_{atom} - \frac{\left\{ \frac{2 C_{g,\lambda} D_{g,\lambda}}{L} + g_{a,\lambda} C_{atom,\lambda} \right\}}{\frac{2 D_{g,\lambda}}{L} + g_{a,\lambda}} \right\} \quad (S15)$$

where $Q_{g,\lambda,surface}$ is the gas flux of a certain gas (λ) between the topsoil and the atmosphere $[g\ m^{-2}\ h]$; g_a is the boundary layer conductance $[m\ h^{-1}]$, $C_{atom,\lambda}$ is the concentration of a certain gas in the

atmosphere [$g\ m^{-3}$]; $C_{g,\lambda}$ is the corresponding gaseous concentration in soil [$g\ m^{-3}$]; $D_{g,\lambda}$ is the gaseous diffusivity of a certain gas in top soil layer [$m^2\ h^{-1}$]. Besides, gasses may also bubble upwards from soil zones in which the total partial pressure of all aqueous gasses exceeds atmospheric pressure,

$$Q_{b,\lambda} = \left\{0, \frac{p}{RT} - \Sigma_\lambda \left(\frac{C_{g,\lambda}}{S'_\lambda f_{t,s,\lambda} M_\lambda}\right)\right\} \times \frac{C_{g,\lambda} V_w}{\Sigma_\lambda \left(\frac{C_\lambda}{S'_\lambda f t_{d,\lambda} M_\lambda}\right)} \quad (S16)$$

where p is the atmospheric pressure [kPa]; R is the gas constant [$kJ\ mol^{-1}K^{-1}$]; T is soil temperature [K]; $Q_{b,\lambda}$ is bubbling flux of a certain gas (λ) [$g\ m^{-2}\ h$]; θ_w is the soil water content [$m^3\ m^{-3}$]. T is the soil temperature [°C]; S'_λ is the Ostwald solubility coefficient of a certain gas at 30 °C [-]; $f_{t,s,\lambda}$ is the temperature dependence function of S'_λ [-]; $C_{g,\lambda}$ is the gaseous concentration of certain gas in soil [$g\ m^{-3}$]; M_λ is the atomic mass of gas [$g\ mol^{-1}$]. V is the volume of the water [$m^3\ m^{-2}$].

Text S4. Root and mycorrhizal water uptake

Root and mycorrhizal water uptake rates (U_w) are calculated from the difference between canopy water potential (ψ_c) and soil water potential (ψ_s) across soil hydraulic resistances (Ω_s) and root hydraulic resistances (Ω_r). Root resistances are calculated from root radial and from primary secondary axial resistivities using root lengths and surface areas from a root system submodel driven by the exchange of nonstructural C, N, and P along concentration gradients generated by uptake vs. consumption of C, N, and P in shoots and roots.

$$U_W = \frac{\psi'_c - \psi'_s}{\Omega_s + \Omega_r + \Omega_a} \quad (S17)$$

$$\psi'_c = \psi_c + z_b \quad (S18)$$

$$\psi'_s = \psi_s - z_l \quad (S19)$$

$$\Omega_s = ln\left\{\frac{d/r}{2\pi L\kappa}\right\} \theta_w/\theta_p \quad (S20)$$

$$\Omega_r = \frac{\Omega'_r}{L} \quad (S21)$$

where U_w is the root water uptake rate [$m^3\ m^{-2}\ h^{-1}$]. Positive values indicate water uptake, and negative values indicate exudation; ψ_c is the canopy water potential, solved along with the canopy energy balance (Grant et al., 1993a). z_b is the length of bole from the soil surface to the top of the canopy [m]. z_l is the depth of the soil layer below the soil surface [m]. L is the length of the roots. Ω'_r is radial resistivity to water transport from the surface to the axis of roots or mycorrhizae, which is a constant value ($1.0 \times 10^4\ MPa\ h\ m^{-2}$). θ_w is the soil water content [$m^3\ m^{-3}$]. θ_p is the soil porosity [$m^3\ m^{-3}$]. Ω_s is the soil hydraulic resistance [$m\ h\ m^{-2}$]. Ω_r is the soil hydraulic resistance [$m\ h\ m^{-2}$]. Ω_a is the axial resistance to water transport along axes of primary or secondary roots or mycorrhizae [$m\ h\ m^{-2}$], determined by the number of primary or secondary axes, the mass of roots or mycorrhizae, and the radius of roots and bole. Detailed representations can be found in the model document on the GitHub.

Text S5. Plant nutrients uptake

The plant nutrient uptake rate in *ecosys* is controlled by both the soil nutrients supply (solute transport rates to root surfaces) and the ability of roots to take up nutrients (active uptake rates at root surface where). Plant uptakes soil nutrients (i.e., NO_2^-, NO_3^-, NH_4^+, and PO_4^{3-}) through root, and the movement of solute to uptake sites at the root surface is assumed to be radical, and the supply rate is calculated with a radial formulation of the convection-dispersion equation,

$$U_{\lambda,s} = U_w C_{\lambda,s} + D_{\lambda,s} \frac{\partial C_{\lambda,s}}{\partial r} \quad (S22)$$

$$U_{\lambda,s} = U_w C_{\lambda,s} + 2\pi D_{\lambda,s} L \frac{C_{\lambda,s} - C_{\lambda,u}}{l\left(\frac{r_D}{r_R}\right)} \quad (S23)$$

$$D_{\lambda,s} = D_q|U_w| + D_\lambda f_{t,s,\lambda} \tau \theta_W \quad (S24)$$

where $U_{\lambda,s}$ is the rate of the nutrient (λ) transfer from soil to the uptake site at the root surface [$g\ m^{-2}\ h^{-1}$]; U_w is the root water uptake rate [$m^3\ m^{-2}\ h^{-1}$]; L is the root length [m]; $C_{\lambda,s}$ is the solute concentration of λ in soil water [$g\ m^{-3}$]; $C_{\lambda,u}$ is the solute concentration of λ at the site of uptake [$g\ m^{-3}$]; r_D is the mean half-distance between adjacent roots [m]. r_R is the root radius [m]; $D_{\lambda,s}$ is the dispersivity-diffusivity of solute λ in the soil during uptake [$m^2\ h^{-1}$], determined by the hydrodynamic dispersion coefficient (D_q) [m], U_w, the solute diffusivity at 0 °C in soil (D_λ) [$m^2 h^{-1}$], temperature dependence function ($f_{t,s,\lambda}$), the soil water-filled porosity (θ_w); τ is the soil tortuosity [-].

Active uptake of the nutrient λ is modeled in the Michaelis-Menten format,

$$U_\lambda = \frac{U'_\lambda\left(C_{\lambda,u} - C'_{\lambda,u}\right)}{\left(C_{\lambda,u} - C'_{\lambda,u}\right) + K_\lambda} \quad (S25)$$

$$U'_\lambda = U'_{\lambda,0} A f_{t,R} f_{o,R} \quad (S26)$$

where U_λ is the active uptake of nutrient λ [$g\ m^{-2}\ h^{-1}$]; U'_λ is the maximum uptake rate of nutrient λ [$g\ m^{-2}\ h^{-1}$], determined by standard maximum uptake rate of nutrient λ ($U'_{\lambda,0}$) [$g\ m^{-2}\ h^{-1}$], root area index (A) [$m^2\ m^{-2}$], temperature dependence function for respiration ($f_{t,R}$) [-], and the oxygen-dependence function for respiration ($f_{o,R}$) [-]; $C_{\lambda,u}$ is the solute concentration of λ at the site of uptake [$g\ m^{-3}$]; $C'_{\lambda,u}$ is the threshold for nutrient λ uptake [$g\ m^{-3}$], below which the uptake rate is 0; K_λ is the Michaelis-Menten constant for root nutrient λ uptake [$g\ m^{-3}$], at which the uptake rate is $U'_\lambda/2$. Equality between $U_{\lambda,s}$ and U_λ is obtained through iterative convergence to a common value of $C_{\lambda,u}$ in the above equations.

Text S6. Root respiration and crop oxygen demand

Root plays a critical role in crop growth by acquiring necessary resources, including water and nutrients (i.e. nitrogen, phosphorus, etc.), from the soil for crop development, and stabilizing crop body structure (Hodge et al., 2009). Understanding the interactive root system and soil is essential to quantify the impacts of different environmental factors on crop growth (Jin et al., 2020). *Ecosys* explicitly simulates the root system with a representation of vertical primary axes and horizontal secondary axes (details in (Grant, 1993, 1998)). In the model, root growth and maintenance are driven by root respiration, and the rate of root respiration at maximum turgor in each soil layer is controlled by the available carbon storage, soil moisture, temperature, oxygen availability, and nutrient status,

$$R_T = Q_R C_R f_{t,R} f_{o,R} f_{\lambda,R} \quad (S27)$$

where R_T is the root respiration for maintenance and growth [$g\ C/m^2/h$]; Q_R is the specific respiration of CH_2O [$g\ /g/h$]; C_R is nonstructural CH_2O in root [$g\ C/m^2$]; $f_{t,R}$ is the temperature function for respiration [-]; $f_{o,R}$ is the oxygen function for respiration, represented as the ratio of O_2 uptake to O_2 demand [-], and will be detailed in the Section 2.1.3 below; $f_{\lambda,R}$ is the nutrient status function for respiration [-]. The actual respiration rate is further adjusted by root turgor and soil strength (Grant, 1993, 1998). Nutrient uptake ($NO_3^-, NH_4^+, PO_4^{3-}$) also respires CH_2O,

$$R_U = \alpha \Sigma U_\lambda \quad (S28)$$

where R_U is the respiration for nutrient uptake [$g\ C/m^2/h$]; α is the specific respiration rate for nutrient uptake [-]; U_λ is the uptake rate of nutrient Z ($NO_3^-, NH_4^+, PO_4^{3-}$) [$g\ N/m^2/h$ or $g\ P/m^2/h$]. The total

root respiration is, then, the total respiration for root maintenance, root growth, and root nutrient uptake ($R_T + R_U$).

The crop oxygen demand (U_O') is defined as the oxygen uptake rate without soil oxygen limits,

$$U_O' = \frac{\frac{R_T}{f_{o,R}} + R_U}{R_Q} \quad (S29)$$

where R_Q is the respiratory quotient [$g\ C/\ (g\ O_2)$].

Text S7. Oxygen uptake and oxygen stress

The oxygen uptake rate in *ecosys* is controlled by both the soil oxygen supply (dissolved oxygen transport rates to root surfaces) and the ability of roots to take up oxygen (active uptake rates at root surface where respiration is modeled). The conceptualization of crop roots is depicted in Figure S1, with a porous core in the middle, surrounded by an aqueous zone where respiration happens, then encased in a water film. Gaseous and dissolved oxygen transport in both the root porous core and the soil contribute to root respiration. The movement of oxygen is assumed to be radial, so the rate of oxygen moving from the soil water to the root surface and the rate of oxygen moving from the aqueous zone of the root porous core to the root surface are obtained from equation (S30) and equation (S31), respectively.

$$U_{O,s} = U_w C_{O_2,s} + 2\pi D_{O_2} L \frac{(C_{O_2,s} - C_{O_2,R})}{lnln\left(\frac{r_R + r_W}{r_R}\right)} \quad (S30)$$

$$U_{O,P} = 2\pi D_{O_2} L \frac{C_{O_2,R} - C_{O_2,P}}{l\left(\frac{r_R}{r_P}\right)} \quad (S31)$$

where $U_{O,s}$ is the rate of oxygen uptake by root from soil [$g/m^2/h$]; $U_{O,P}$ is the rate of oxygen uptake by root from the root porous core [$g/m^2/h$]; U_w is the root water uptake rate [$m^3/m^2/h$], determined by soil and root water potential and root resistances (R. F. Grant, 1998); D_{O_2} is the dispersivity-diffusivity of dissolved oxygen [$m^2\ h^{-1}$] (Bresler, 1973); L is the root length [$m\ m^{-2}$]; $C_{O_2,s}$ is the dissolved oxygen concentration in the soil [$g\ m^{-3}$]; $C_{O_2,R}$ is the oxygen concentration at the respiration site [$g\ m^{-3}$]; $C_{O_2,P}$ is the dissolved oxygen concentration in the root porous core [$g\ m^{-3}$]; r_R is root radius [m]; r_W is the thickness of the water film [m] (Kemper & Rollins, 1966); r_P is the radius of the root porous core [m]. The active oxygen uptake rate by roots is modeled in the Michaelis-Menten format,

$$U_O = \frac{U_O' C_{O_2,R}}{C_{O_2,R} + K_O} \quad (S32)$$

where U_O is the root oxygen uptake rate [$g/m^2/h$], K_O is the Michaelis-Menten constant for root oxygen uptake [$g\ m^{-3}$]. U_O is solved iteratively from equations (30-32), with $U_O = U_{O,s} + U_{O,P}$. All dissolved oxygen concentrations are driven by oxygen transport in gaseous phases and by dissolution from gaseous to aqueous phases in soil and roots, which will be affected by soil drainage conditions. Details of oxygen transport and dissolution (i.e. aqueous and gaseous) in soil and root can be found in (R. F. Grant, 1993). Then, the oxygen stress indicator ($f_{o,R}$) in equation (3) is defined as the ratio between the U_O and U_O'

$$f_{o,R} = \frac{U_O}{U_O'} \quad (S33)$$

Text S8. Heterotrophic microbial activity

The soil C, N, and P transformation (e.g., hydrolysis, nitrification-denitrification, fermentation, methanogens, mineralization- immobilization, etc.) in the soil is regulated by microbial activities in six organic states (i.e., solid organic matter, soluble organic matter, sorbed organic matter, acetate, microbial communities, and microbial residues) in *ecosys* (Grant et al., 1993b, c). Each organic state contains four organic matter-microbe complexes: plant litterfall, animal manure, particulate organic matter, and humus. Microbes are the agents of organic matter transformation and the abundance of each microbe functional type (e.g., aerobic bacteria, denitrifiers, fungi, fermenters + acetogens, acetotrophic methanogens, NH_4^+ oxidizers, NO_2^- oxidizers, methanotrophs, hydrogenotrophic methanogens) regulate the transformation rates (Grant and Pattey, 2003), and each microbial functional type in each complex is further classified into three kinetic components (i.e., labile, resistant, storage) with different reaction rates.

In this part, we present the formula related to heterotrophic nitrifier microbial functional types (i.e., obligately aerobic heterotrophs and facultatively anaerobic heterotrophs) to illustrate the dynamics of soil microbes and the role of oxygen in regulating its activities. In *ecosys*, organic substrates (i.e., solid organic matter and microbial residues) will first be hydrolyzed and transformed into soluble organic matter. **The heterotrophic functional types will, on the one hand, oxidize the soluble organic matter and regulate the C, N, and P transformation. On the other hand, the oxidation will provide essential nutrients and energy for the maintenance and growth of heterotrophic functional types**. In this process, the heterotrophic nitrifier functional types will first use the soil oxygen as the oxidizing agent, and NO_3^-, NO_2^-, N_2O will be reduced sequentially if the demand for electron acceptors is unmet. Similar to root oxygen uptake, **the microbe's oxygen uptake is determined by both the complex oxygen demand and the soil oxygen supply**. The demand for O_2 reduction is determined by the biomasses of the heterotrophic functional types (heterotrophs) and the concentration of soluble organic matter,

$$X'_{C_{i,h}} = \frac{X'_{C_h} M_{i,h,a} C_{W_{i,C}}}{K_{Rh} + C_{W_{i,C}}} f_{t,m} \quad (34)$$

$$R'_{O_2 i,h} = RQ_C X'_{C_{i,h}} \# (35)$$

where $W_{i,C}$ represents a type of soluble organic carbon, and the subscript i denotes different organic matter-microbe complexes; $C_{W_{i,C}}$ is the concentration of $W_{i,C}$ [$gC\ m^{-3}$]. $X'_{C_{i,h}}$ is the oxidation of $W_{i,C}$ coupled to the reduction of O_2 under saturated soil [$gC\ m^{-2}\ h^{-1}$]. X'_{C_h} is the specific oxidation of $W_{i,C}$ at saturated $W_{i,C}$ at 30 °C [$gC\ gC^{-1}h^{-1}$]. $M_{i,h,a}$ is the active biomass of heterotrophs [$gC\ m^{-2}$]; K_{Rh} is the Michaelis-Menten constant for the reduction of $W_{i,C}$ by heterotrophs [$gC\ m^{-3}$]; $f_{t,m}$ is the temperature function for microbial processes [-]; $f_{w,m}$ is the water stress function for microbial processes [-]; $R'_{O_2 i,h}$ is the rate of soil O_2 reduction by heterotrophs without the oxygen limitation [$gO_2\ m^{-2}h^{-1}$]; RQ_C is the respiratory quotient for reduction of O_2 coupled to oxidation of C (=2.67). The O_2 uptake by microbial functional types is then modeled in the Michaelis-Menten format,

$$R_{O_2,i,h} = \frac{R'_{O_2 i,h} C_{O_2,m}}{C_{O_2,m} + K_{O_2 h}} \quad (36)$$

where $C_{O_2,m}$ is the O_2 concentration at the microbe surfaces [$gO_2\ m^{-3}$]; $R_{O_2,i,h}$ is the O_2 reduction (uptake) by heterotrophs under $C_{O_2,m}$ [$gO_2\ m^{-2}h^{-1}$]; $K_{O_2 h}$ is the Michaelis-Menten constant for the oxidation of O_2 [$gO_2\ m^{-3}$]. The movement of oxygen to each functional type is assumed to be spherical, and the rate of oxygen moving from the soil water to the functional type is given by the spherical convective-dispersive equation,

$$R_{O_2,i,h} = 4\pi n D_{O_2} \frac{r_m r_s}{r_s - r_m} \left(C_{O_2,s} - C_{O_2,m}\right) \quad (37)$$

where D_{O_2} is the dispersivity-diffusivity of dissolved oxygen [m^2h^{-1}]; r_m is the radius of the microbial sphere [m]; r_s is the radius of the microbial sphere plus the thickness of the water film [m]; $C_{O_2,s}$ is the dissolved oxygen concentration in the soil [$g\ m^{-3}$]; $C_{O_2,s}$ is the dissolved oxygen concentration at the microbial surface [$g\ m^{-3}$]. $R_{O_2,i,h}$ and $C_{O_2,m}$ are solved with equation (36) and (37).
If the microbe function type is facultatively anaerobic heterotrophs (using subscript d here, as a subset of h, above), additional respiration is enabled through the sequential reduction of ${NO_3}^-$, ${NO_2}^-$, and N_2O.

$$R_e = 0.125\left(R'_{O_2,i,d} - R_{O_2,i,d}\right) \tag{38}$$

$$R_{NO_3^-,i,d} = 7R_e \frac{C_{NO_3^-}}{C_{NO_3^-} + K_{NO_3^-,d}} \tag{39}$$

$$R_{NO_2^-,i,d} = \left(7R_e - R_{NO_3^-,i,d}\right)\frac{C_{NO_2^-}}{C_{NO_2^-} + K_{NO_2^-,d}} \tag{40}$$

$$R_{N_2O,i,d} = 2\left(7R_e - R_{NO_3^-,i,d} - R_{NO_2^-,i,d}\right)\frac{C_{N_2O}}{C_{N_2O} + K_{N_2O,d}} \tag{41}$$

where R_e is the electron transfer to N oxides by denitrifiers [$mol\ e^-\ m^{-2}h^{-1}$]; $R_{NO_3^-,i,d}$, $R_{NO_2^-,i,d}$, and $R_{N_2O,i,d}$ are the ${NO_3}^-$, ${NO_2}^-$, and N_2O reduction by denitrifiers, respectively [$gN\ m^{-2}h^{-1}$]; $C_{NO_3^-}$, $C_{NO_2^-}$, and C_{N_2O} are the concentrations of ${NO_3}^-$, ${NO_2}^-$, and N_2O, respectively [$gN\ m^{-3}$]. The energy generated in oxidation will first be used for microbial maintenance and growth. Meanwhile, each microbial functional type undergoes first-order decomposition (Grant et al., 1993c).

Text S9. Drought numerical experiment

With climate change, the U.S. Midwest is expected to experience wetter springs and drier summers, with more frequent and intense late-spring storms and severe summer droughts (Lesk et al., 2016; Li et al., 2019; Lobell et al., 2014; Schmidhuber and Tubiello, 2007; Seneviratne et al., 2022; Zhou et al., 2022). We are particularly interested in investigating the potential of tile drainage under climate change in this study, and we found that the benefits of tile drainage under climate change could be in two folds: 1) tile drainage directly benefits crop growth under excessive spring precipitation, as exemplified by the results in 2009 and 2010 (Figure 10 and S14). 2) The developed root system helps to mitigate the drought impact during summer, as exemplified by the simulation results in 2013. However, the second point is not intuitive due to the complex weather conditions. In this part, we will have a deeper discussion to show the benefits of tile drainage in 2013, along with a hypothetical numerical experiment demonstrating crops did experience drought stress in 2013.

The planting date in 2013 is 12th June 2013, and the field receives abundant rainfall in April and May, which provided excessive soil water during the early growing stage while experiencing severe drought in June, July, and August (Figure S8). Overall, we could observe a significant yield reduction in 2013 compared with other soybean years (Figure S13). Due to its complex weather conditions, two reasons might induce the yield reduction: 1) excessive water in the early growing stage; and 2) drought in the summer. To demonstrate the crop suffering drought stress, we here performed a hypothetical numerical experiment by replacing the climate drivers (e.g., precipitation) from June to August in 2013 with those in 2008. Figure S9 suggests that the precipitation from June to August in 2008 is close to the average values. Figure S15 shows the model simulated water fluxes. The field receives more precipitation and more surface runoff, subsurface discharge, and ET are generated in the hypothetical scenario. The hypothetical scenario yields the highest grain carbon and gross primary production (GPP) compared with both tile and no-tile conditions with real climate drives (Figure S16), which suggests drought stress negatively affects

crop yield. Figure S17 suggests that, at the early growing stage, the hypothetical numerical experiment with more precipitation suffers more soil oxygen stress, indicated by the smaller values of the crop's actual O_2 uptake rate to O_2 demand under non-limiting O_2 conditions. Meanwhile, crops suffer less water stress (drought) from June to August, indicated by less negative minimum canopy water potential. In summary, more precipitation in the hypothetical experiment leads to higher O_2 stress at the early growing stage, while it mitigates water (drought) stress. Ultimately, more precipitation increases crop yield, which demonstrates that drought stress is a critical factor that reduces crop yield in 2013.

Supplemented figures

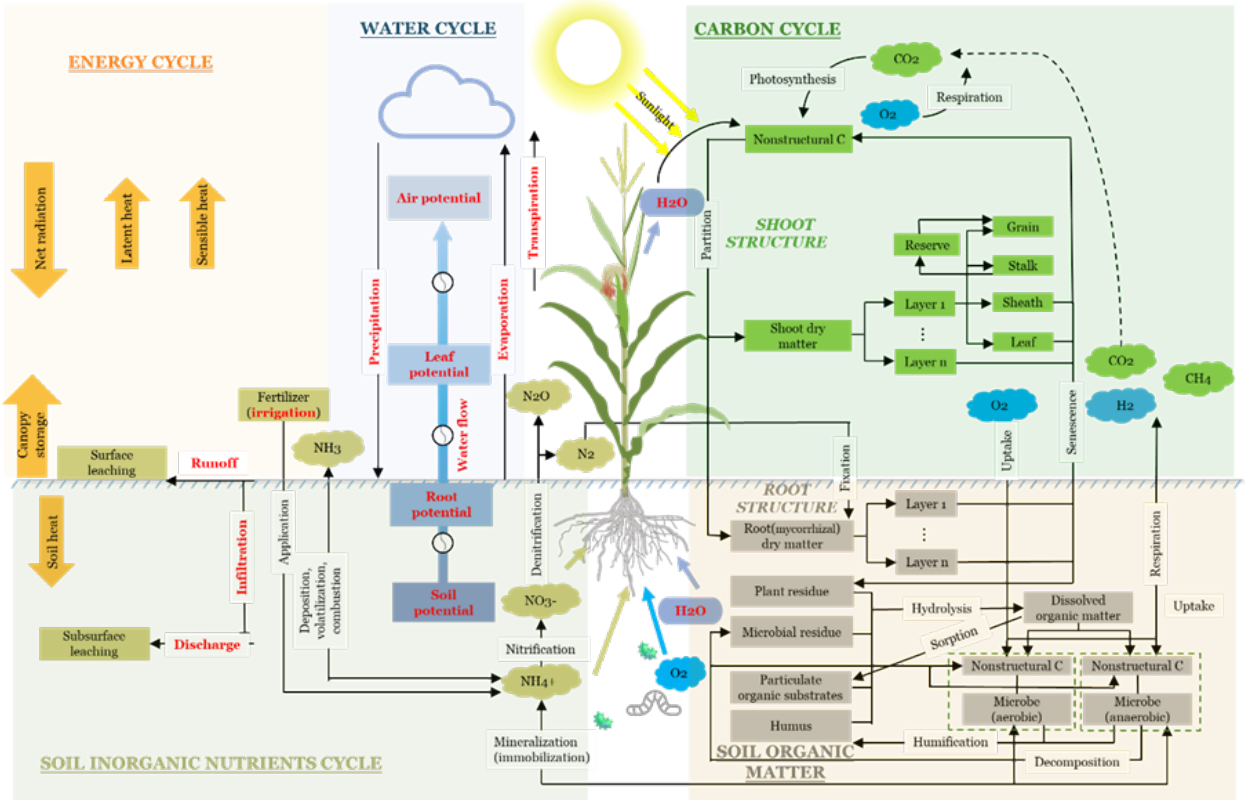

Figure S1. Schematic of the processes in *ecosys*. Hydrological processes are highlighted with **bold red** fonts.

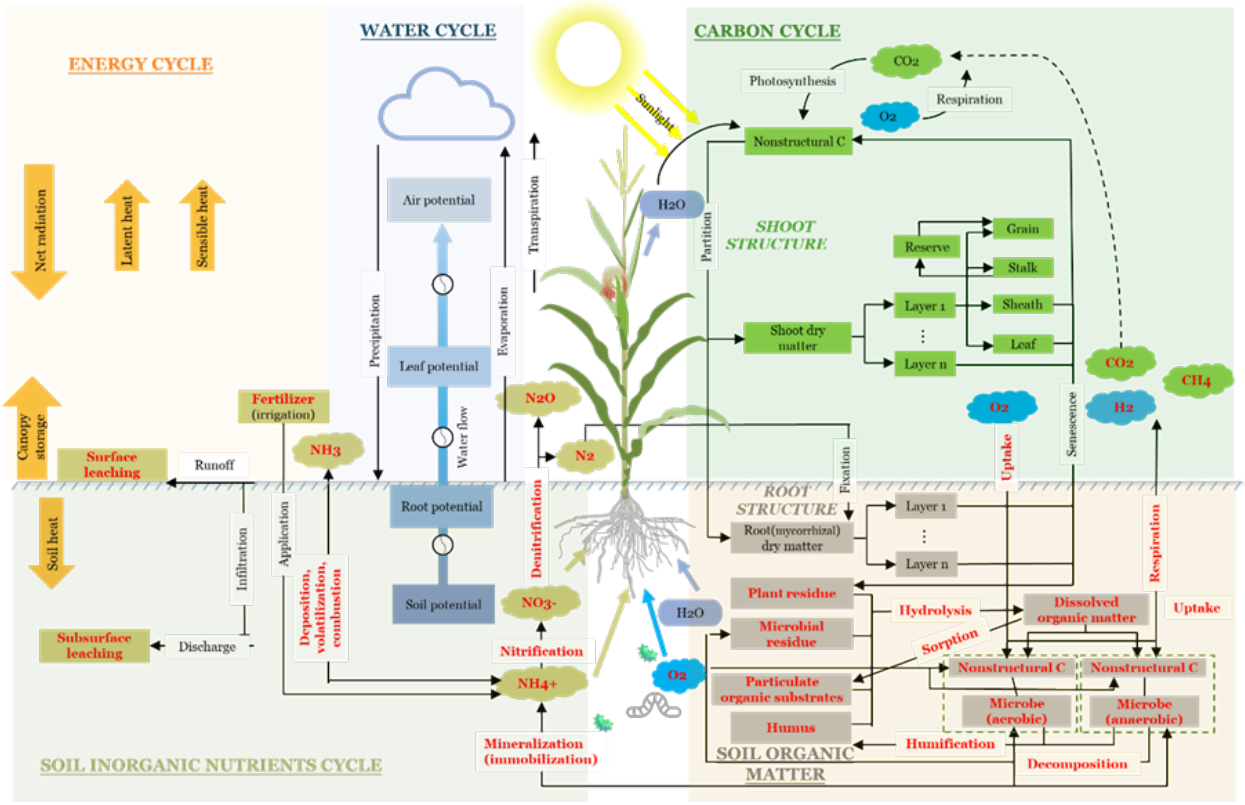

Figure S2. Schematic of the processes in *ecosys*. Soil biogeochemistry-related processes are highlighted with **bold red** fonts.

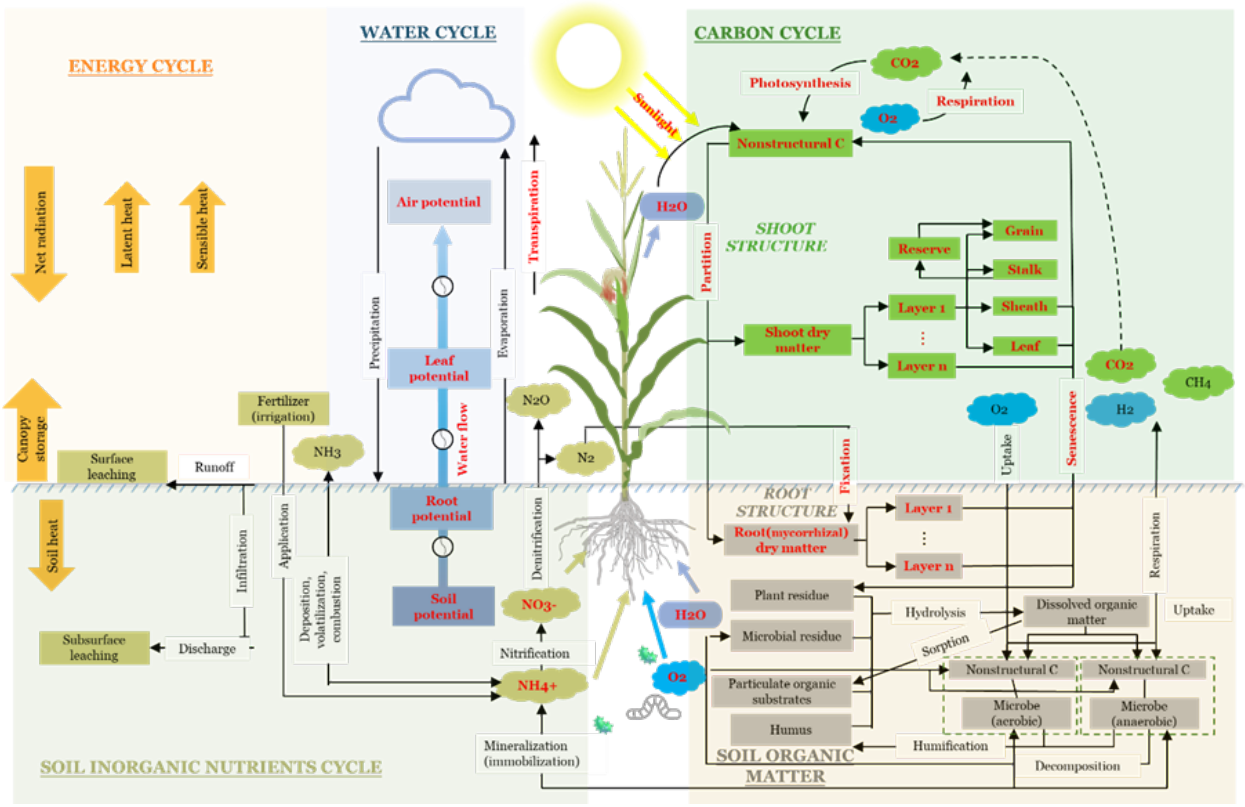

Figure S3. Schematic of the processes in *ecosys*. Plant growth related processes are highlighted with **bold red** fonts.

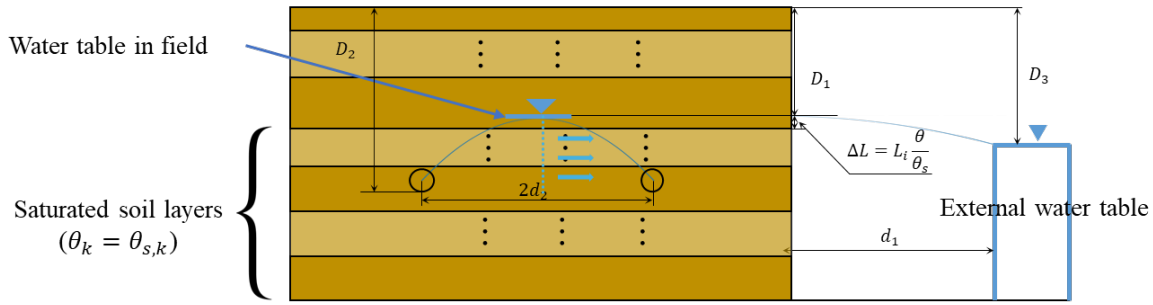

Figure S4. Representation of subsurface water flow. D_1: Water table depth in the field $[m]$; D_2: Tile depth $[m]$; D_3: External water table depth $[m]$; d_1: Distance to the external water table $[m]$; $2d_2$: Tile spacing $[m]$; θ_k: Soil water content in kth soil layer $[m^3/m^3]$; $\theta_{s,k}$: Saturated soil water content in kth soil layer $[m^3/m^3]$; L_i: The thickness of the ith soil layer $[m]$.

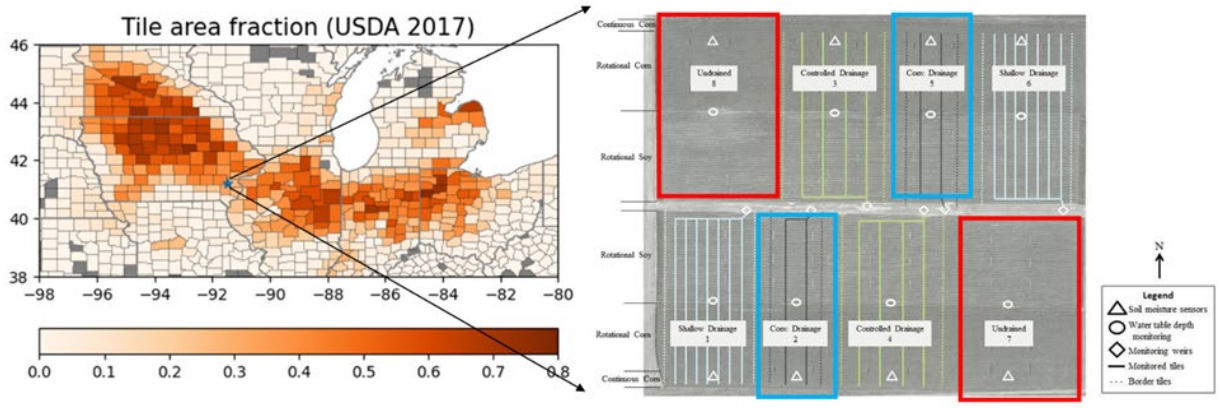

Figure S5. Tile fractions over the U.S. Midwest region, and the location and layout of the selected experiment field. Red boxes represent sub-fields without tile drainage, and blue boxes represent sub-fields with conventional drainage. This figure is adapted from the ISU transforming drainage dataset (Chighladze et al., 2021; NASS-USDA, 2017).

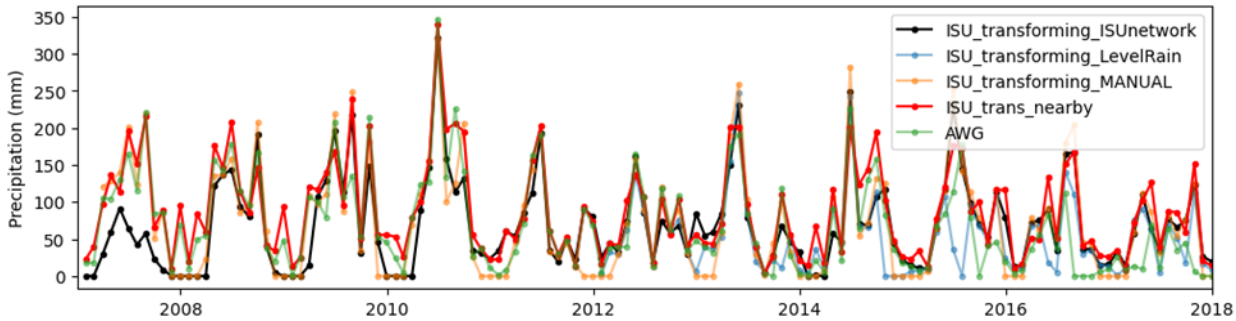

Figure S6. Monthly precipitation from multiple sources near/at the field experiment sites. ***ISU_transforming_ISUnetwork***, ***ISU_transforming_LevelRain***, ***ISU_transoforming_MANUAL***: Precipitation data directly from ISU_transforming drainage dataset associated with the selected site, IA_Washington. ***ISU_trans_nearby***: Precipitation records from a nearby weather station of Iowa Environmental Mesonet, with daily data automatically extracted via https://datateam.agron.iastate.edu/td/dl/#tab_wxdata. ***AWG***: Precipitation records from a nearby weather station of IA_ASOS. To better capture the climate variability, we used an in-situ precipitation dataset to drive the *ecosys* model. Specifically, we mainly used the *ISU_transforming_ISUnetwork* data set as the model input, as *ISU_transforming_ISUnetwork* is the most complete among the three in-situ datasets. However, we found the precipitation in *ISU_transforming_ISUnetwork* is significantly lower than the precipitation in other sources in the comparison between different data sources as shown in this figure. Thus, the precipitation of 2007 is replaced with the NLDAS-2 dataset, with hourly precipitation records.

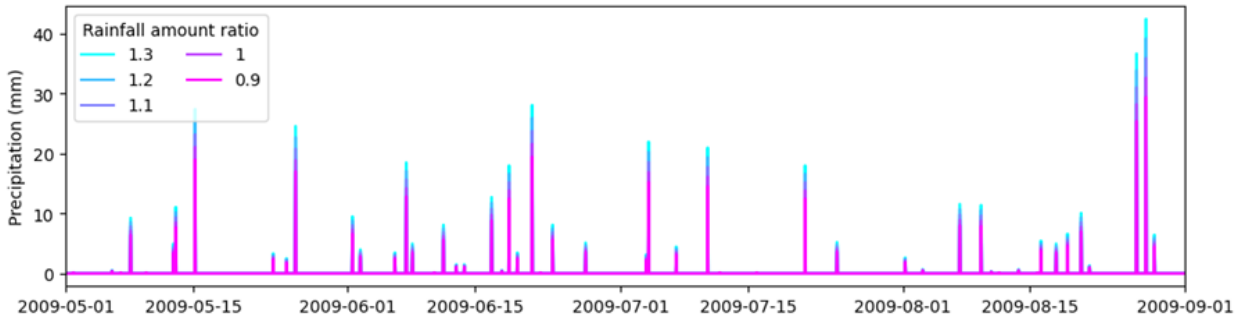

Figure S7. Example of precipitation inputs in numerical experiments. Basically, we changed the precipitation on each time step with a scaling factor (i.e., 0.9, 1, 1.1, 1.2, and 1.3) to account for the increased rainfall intensity.

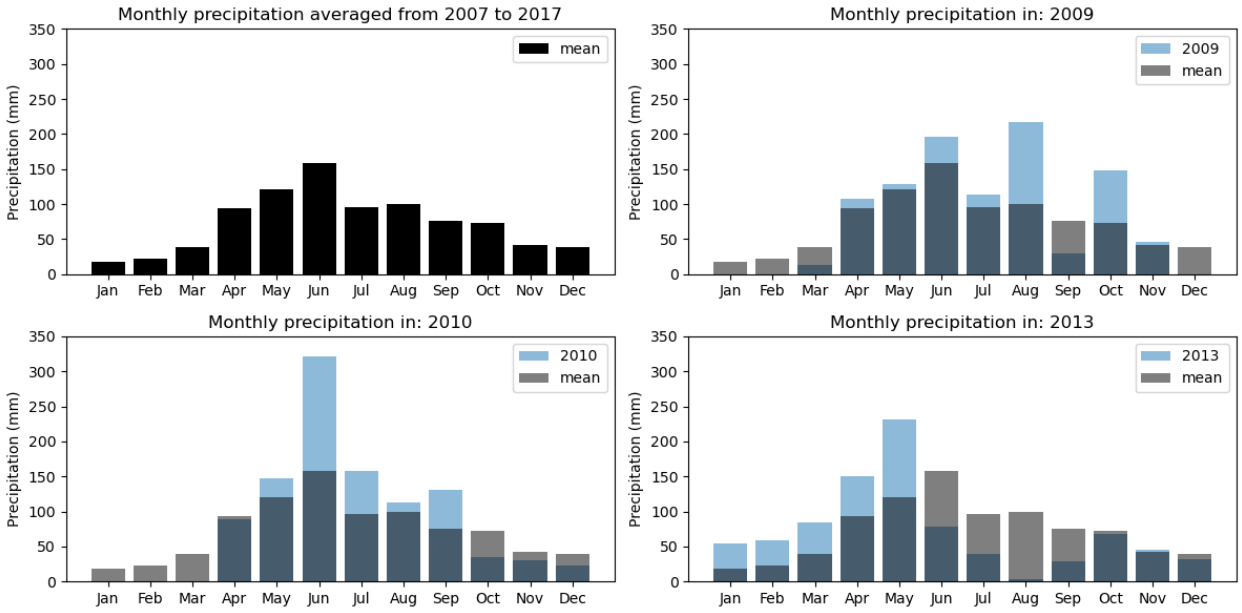

Figure S8. Monthly precipitation. a) Monthly precipitation averaged from 2007 to 2017; **b)** Monthly precipitation in 2009; **c)** Monthly precipitation in 2010; **d)** Monthly precipitation in 2013.

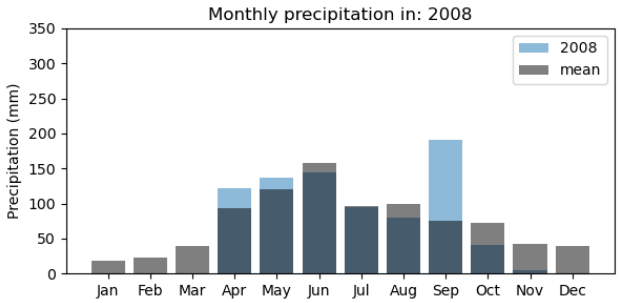

Figure S9. Monthly precipitation in 2008.

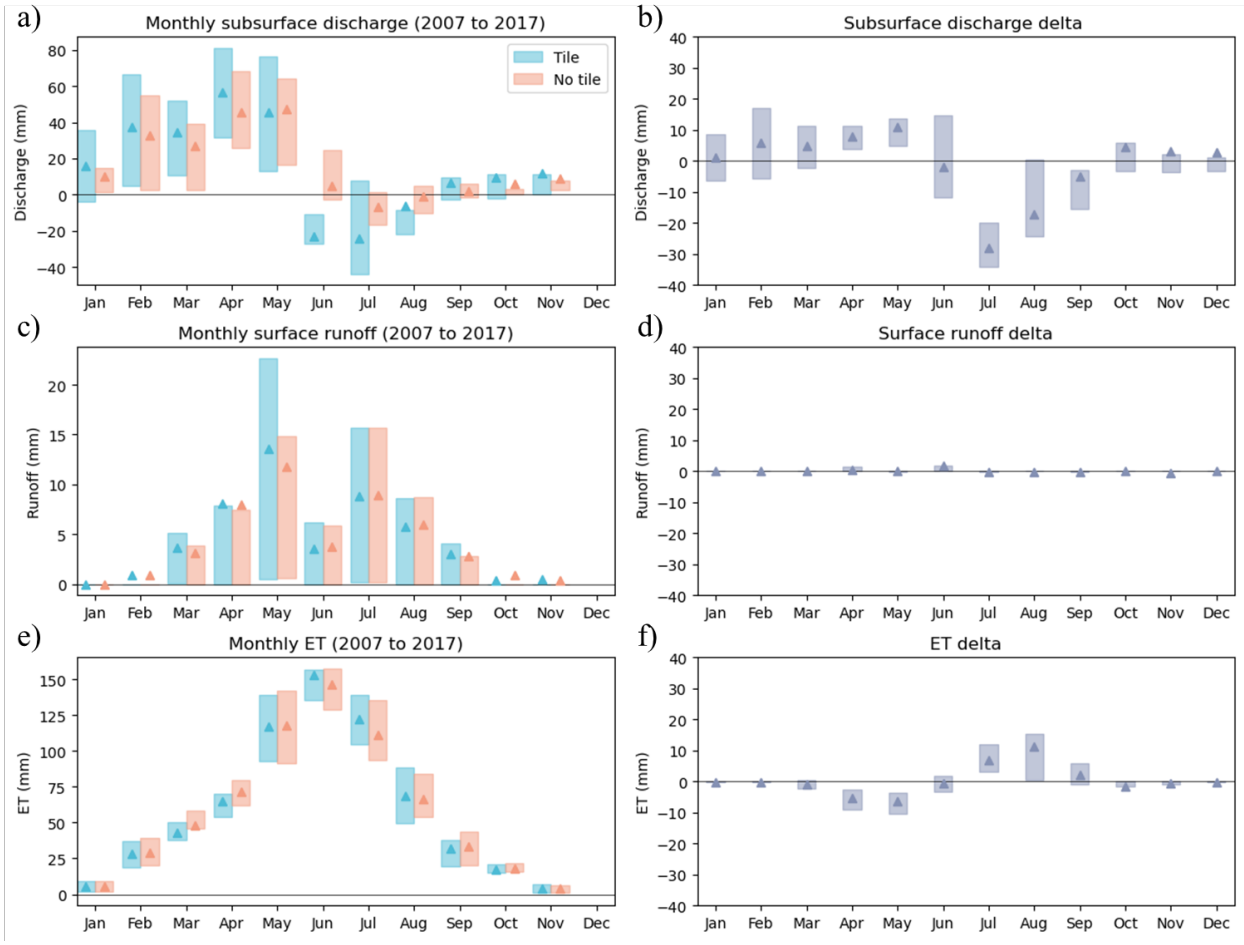

Figure S10. ***Ecosys*-simulated water fluxes under tile and no-tile conditions (2007-2017). a**) Boxplot of the monthly net subsurface discharge (subsurface discharge - subsurface recharge); **b**) Boxplot of the monthly net subsurface discharge difference between tile and no-tile conditions; **c**) Boxplot of the monthly surface runoff; **d**) Boxplot of the monthly surface runoff difference between tile and no-tile conditions; **e**) Boxplot of the monthly ET, **f**) Boxplot of the monthly ET between tile and no-tile conditions. The upper and lower parts of the boxplots indicate 25% and 75% quantiles, and the boxes indicate the interquartile variation. The triangles indicate the mean values. Delta is the difference between tile and no tile conditions.

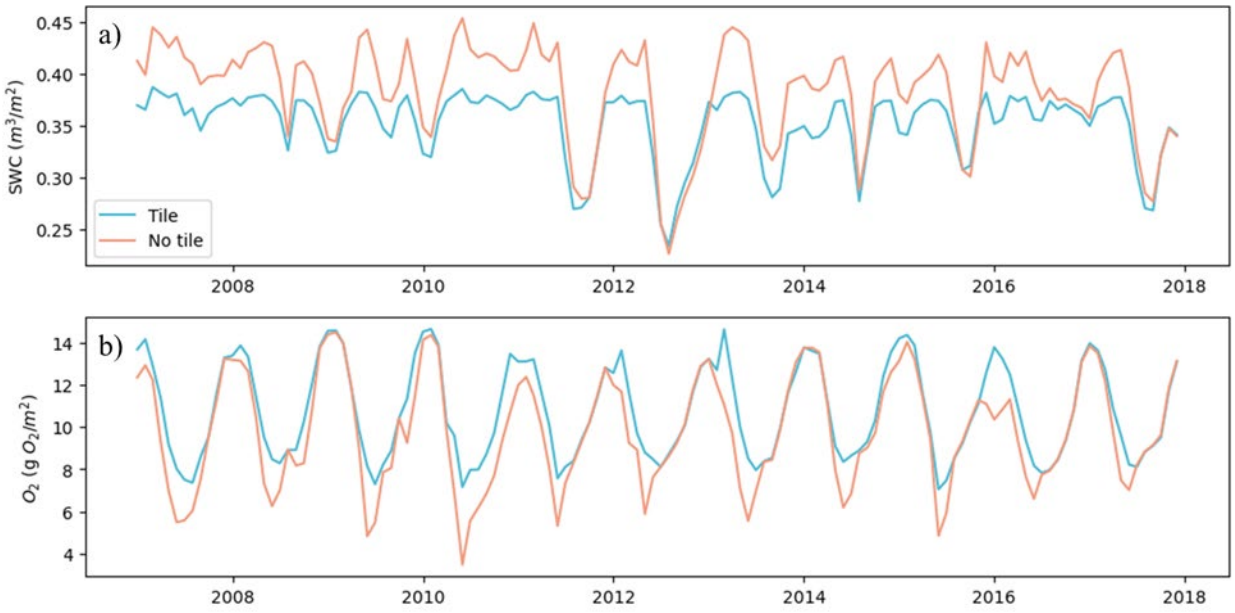

Figure S11. Monthly time series of a) soil water content and b) O2 content in the upper 1 m soil columns.

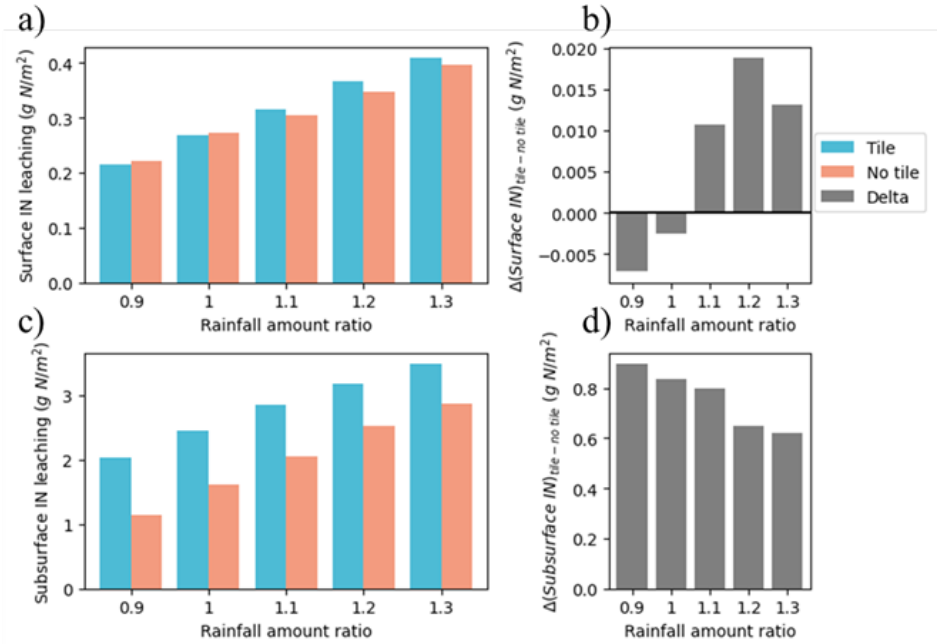

Figure S12. ***ecosys*****-simulated inorganic nitrogen (IN) leaching in the hypothetical numerical experiment under different precipitations. a)** Multiyear surface IN leaching average under tile and no tile conditions**. b)** The tile-induced surface IN leaching increasing (surface IN leaching difference between tile and no tile conditions)**. c)** Multiyear subsurface IN leaching average under tile and no tile conditions**. d)** The tile-induced subsurface IN leaching increasing (subsurface IN leaching difference between tile and no tile conditions).

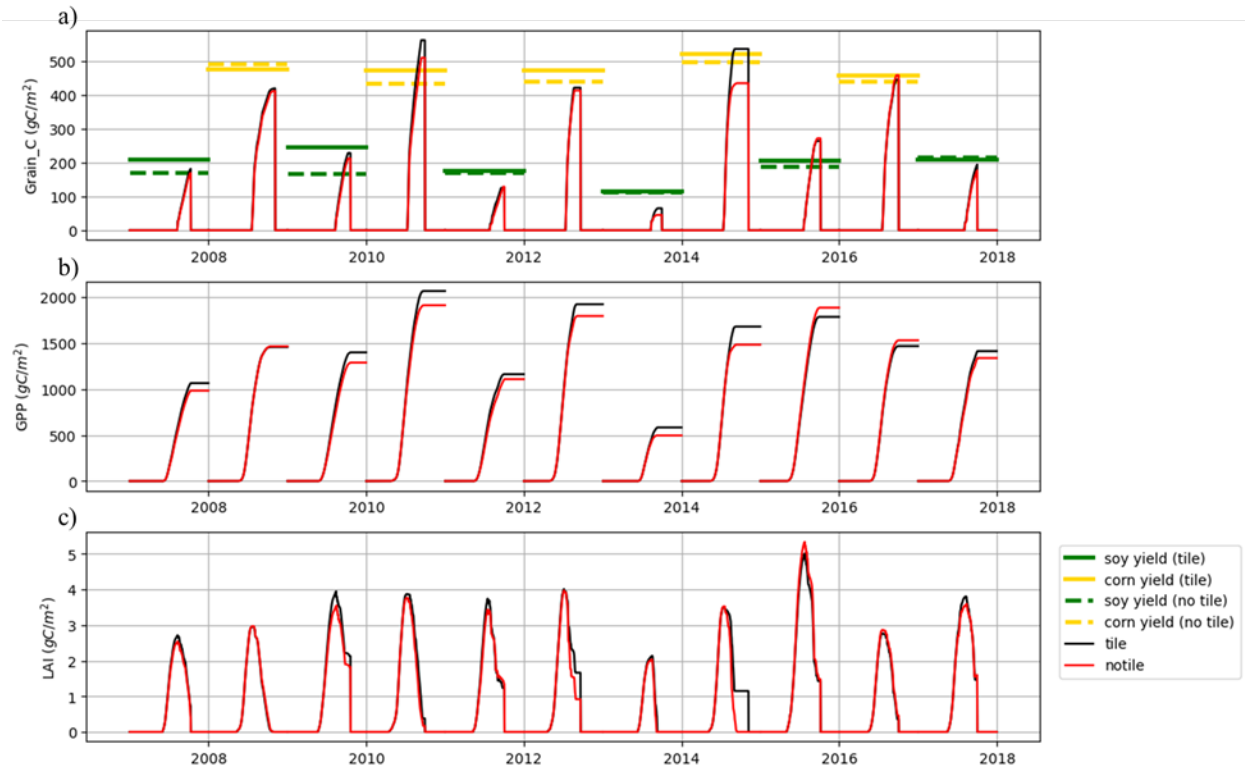

Figure S13. ***Ecosys*****-simulated a) grain carbon, b) GPP, c) LAI.**

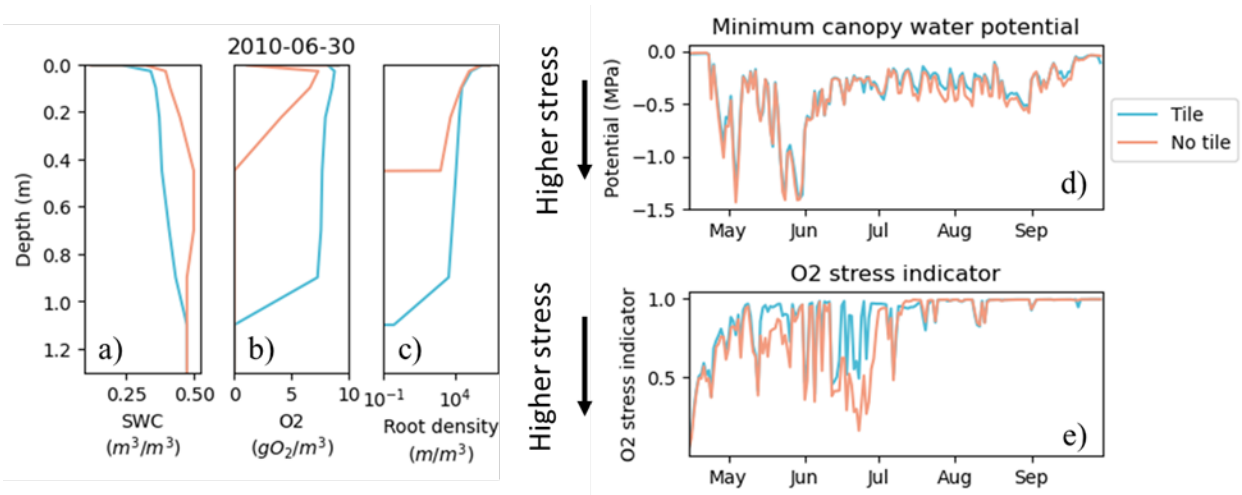

Figure S14. *Ecosys*-simulated soil profile and time series of water and oxygen stress in typical wet corn year. The profile of **a)** Soil water content, **b)** O2 concentration, and **c)** root density profiles in the soil column on June 30th, 2010. Time series of **d)** minimum canopy water potential and **e)** O2 stress indicator (actual O2 uptake rate/potential O2 uptake rate under non-limiting O2 condition) in 2010 (a typical wet year for corns).

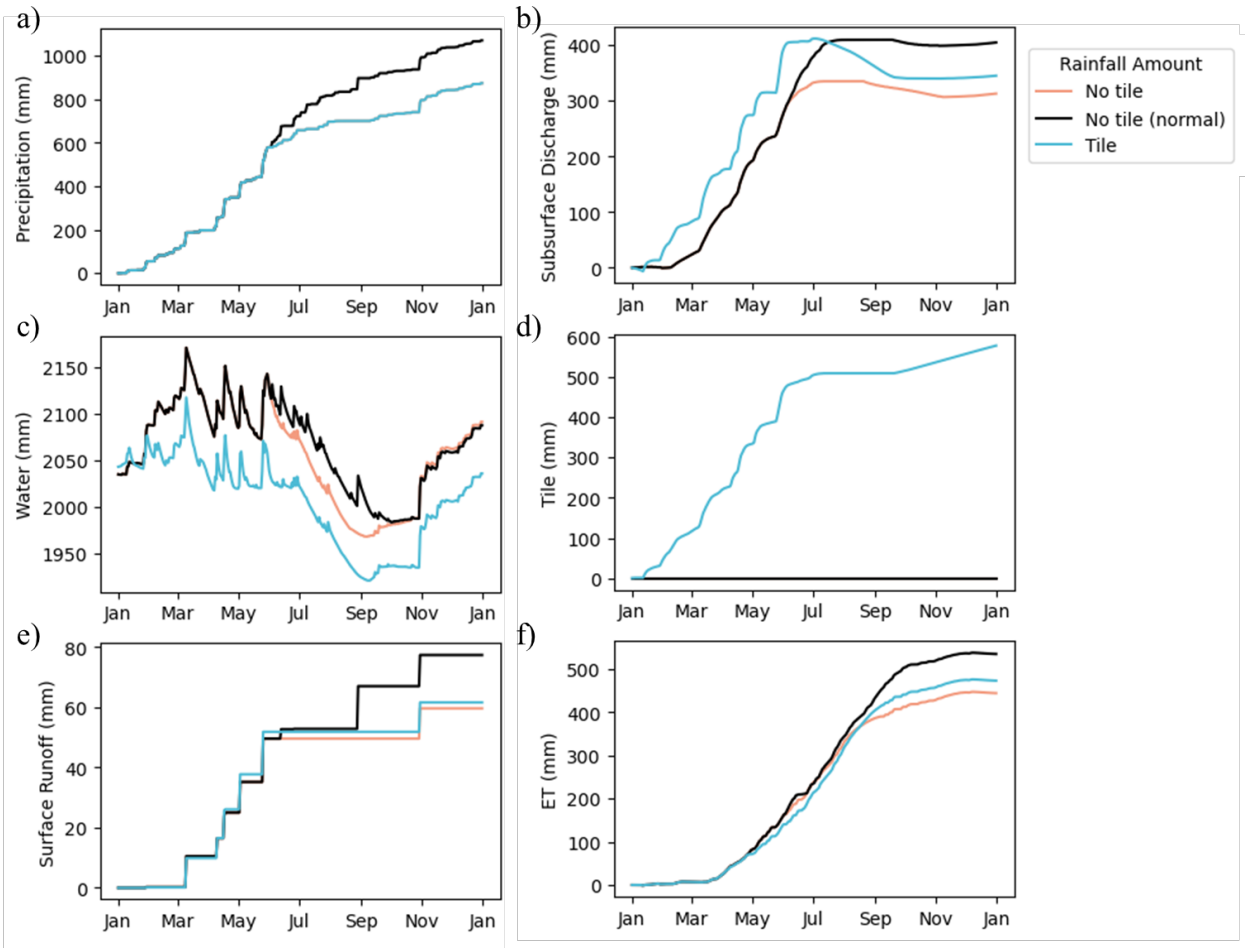

Figure S15. *Ecosys*-simulated water fluxes in 2013. a) Accumulate precipitation. b) Accumulate net subsurface discharge. c) Total soil water content. d) Accumulate tile flow. e) Accumulate surface runoff. f) Accumulated evapotranspiration (ET). The *tile* and *no tile* conditions are driven by the actual climate data from the NLDAS2 dataset and in-situ measurements. The climate forcing in June, July, and August are replaced with those in 2008 under the *no tile (normal)* conditions.

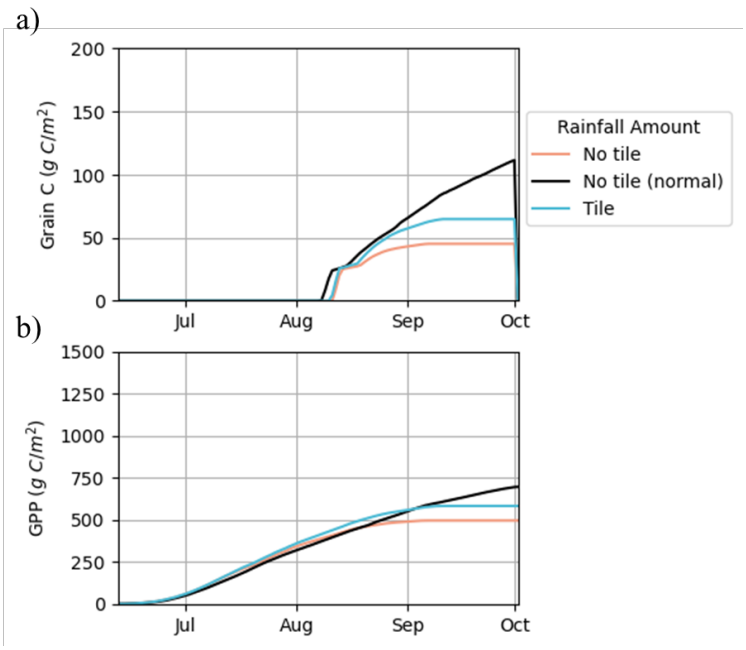

Figure S16. *Ecosys*-simulated a) grain carbon and b) gross primary productivity (GPP) in 2013. The *tile* and *no tile* conditions are driven by the actual climate data from the NLDAS2 dataset and in-situ measurements. The climate forcing in June, July, and August are replaced with those in 2008 under the *no tile (normal)* conditions.

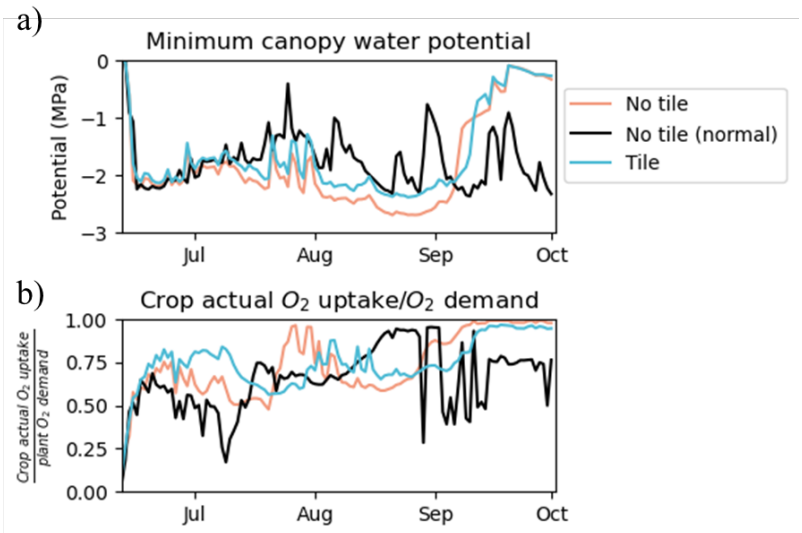

Figure S17. ***Ecosys*-simulated time series of water and oxygen stress in 2013. a**) minimum canopy water potential and **b**) crop actual O2 uptake rate/O2 demand (potential O2 uptake rate under non-limiting O2 condition) in 2009 The *tile* and *no tile* conditions are driven by the actual climate data from the NLDAS2 dataset and in-situ measurements. The climate forcing in June, July, and August are replaced with those in 2008 under the *no tile (normal)* conditions.

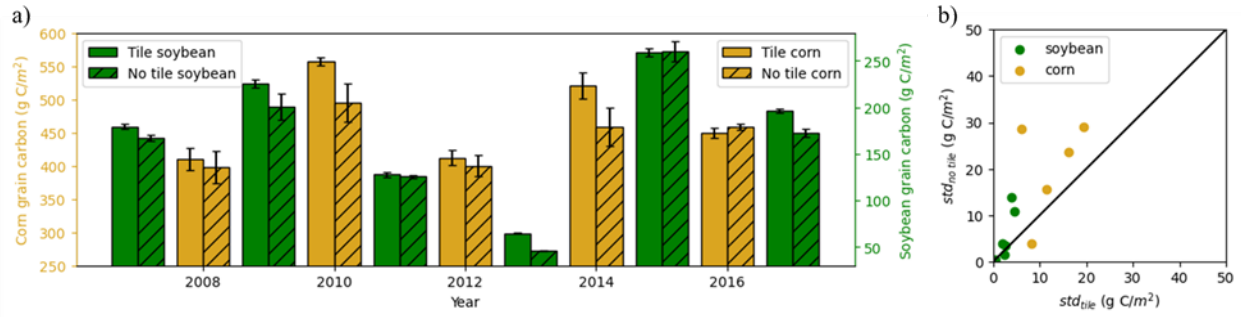

Figure S18. Ecosys simulated crop yield in the hypothetical numerical experiment under different precipitations. a) The mean grain carbon under different precipitation amounts for tile and no-tile conditions. The error bar is the standard deviation of grain carbon under different precipitation amounts for each year. **b**) The comparison between the standard deviation of grain carbon under different precipitation amounts in tile and no-tile conditions.

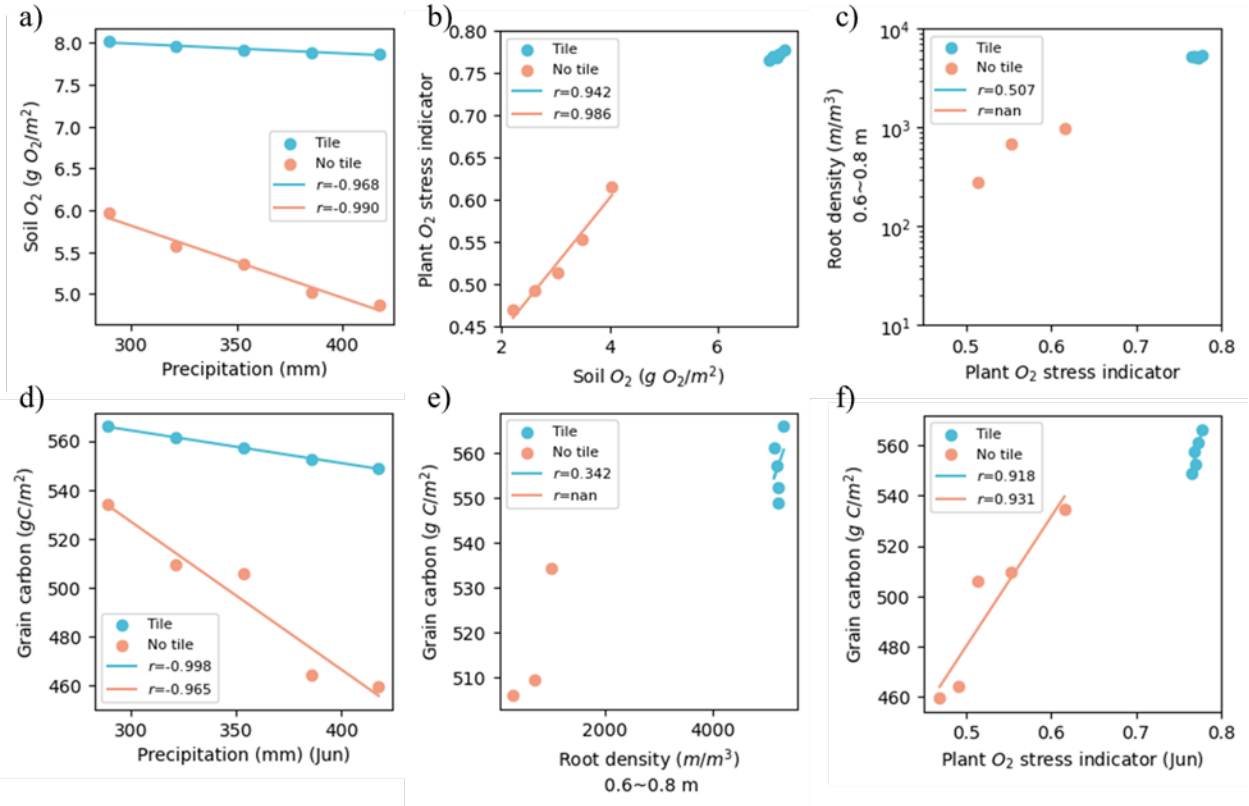

Figure S19. Ecosys-simulated responses of biogeochemistry and plant growth to precipitation amounts in a typical wet year for corn (2010) under tile and no-tile conditions. The relationships between **a)** soil oxygen concentration in the top 1m soil column and precipitation in June, **b)** plant O2 stress indicator and O2 concentration in the top 1m soil column in June, **c)** root density (0.6 m~ 0.8m soil layer) and plant O2 stress indicator in June, **d)** grain carbon and precipitation in June, and **e)** grain carbon and root density (0.6 m~ 0.8m soil layer) in June, **f)** grain carbon and plant O2 stress indicator in June. Figure S7c suggests that under high plant O2 stress, indicated by small values of plant O2 stress indicator, root depths are shallower than 0.6 m.

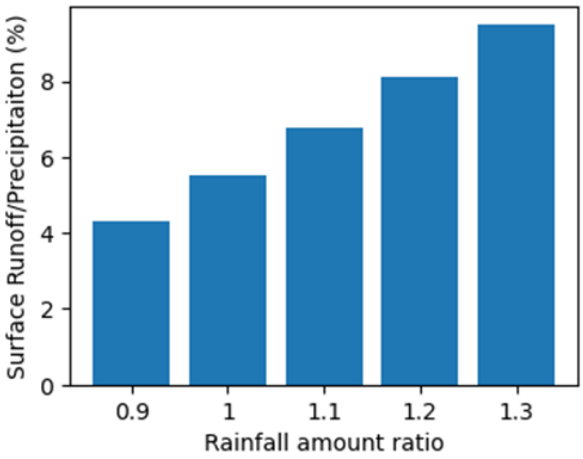

Figure S20. The ratio of surface runoff to precipitation in the hypothetical numerical experiment under different precipitations. With the increase of precipitation amount/intensity, more water leaves the system via surface runoff.

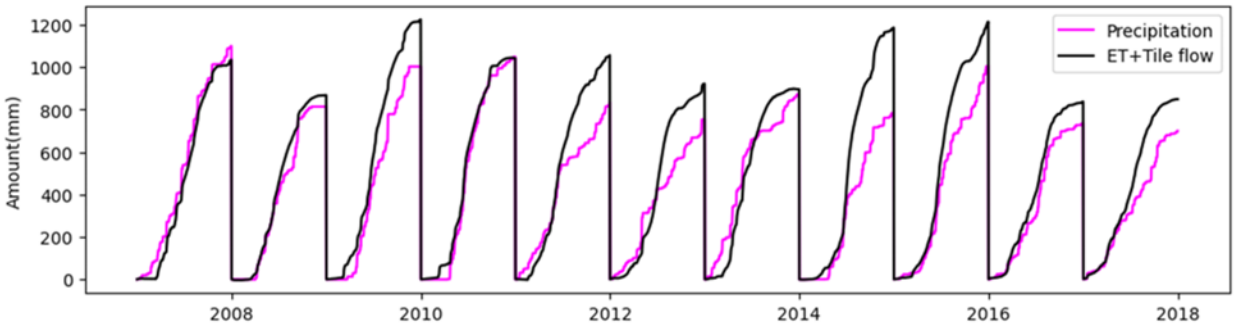

Figure S21. Cumulative precipitation and cumulative *ecosys*-simulated ET+observed tile flow. The results suggested that the precipitation can't sustain both tile flow and field evapotranspiration and recharge from an external source is required to close the system water balance.

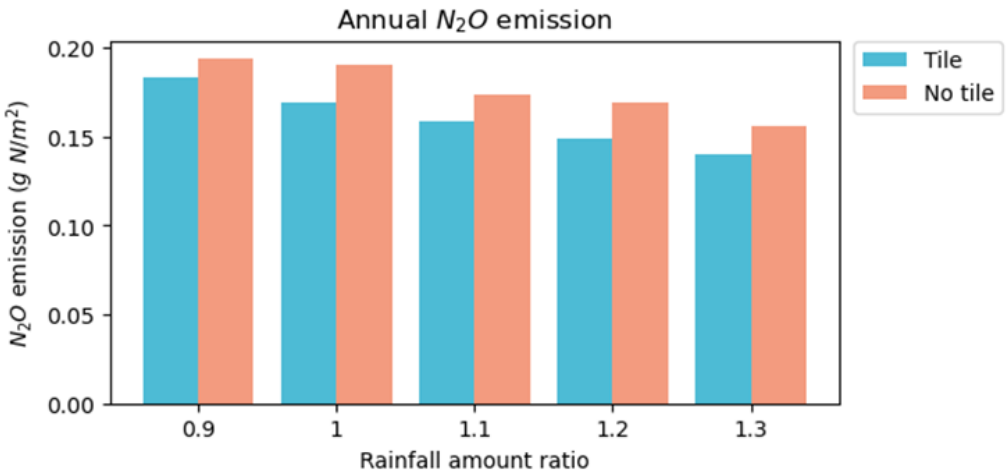

Figure S22. Ecosys-simulated N2O emission under tile and no tile conditions. The results suggested that tile drainage might help to reduce N2O emissions. Besides, the results also suggest that with the increase of precipitation, N2O emission decreases. We hypothesize that soil inorganic substrate decreases with the increase of precipitation, which further leads to less N2O emission under high precipitations.

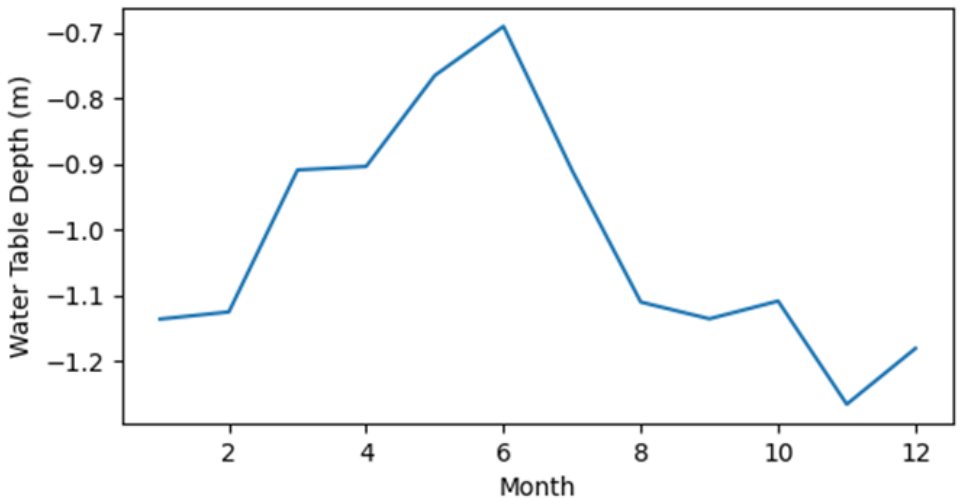

Figure S23. Monthly mean water table depth in no-tile fields. The observation suggested that the water table depth exhibits a seasonal variation. The field water table is shallow in spring, corresponding to high precipitation in those months (Figure S6). In summer, the field water table quickly drops. The field water table reaches the lowest level in November and December. Specifically, the mean water table in January and February in the no-tile field is above the tile pipe, the depth of which is 1.22m. This suggests the possibility of tile flow during these two months, although direct observations of such flow are lacking. A previous study in a nearby watershed, Walnut Creek watershed, also reported tile flow in those two months(Jaynes et al., 1999). Thus, we hypothesized that it might be the low temperature that disabled the measurement devices or no measurement during those two months.

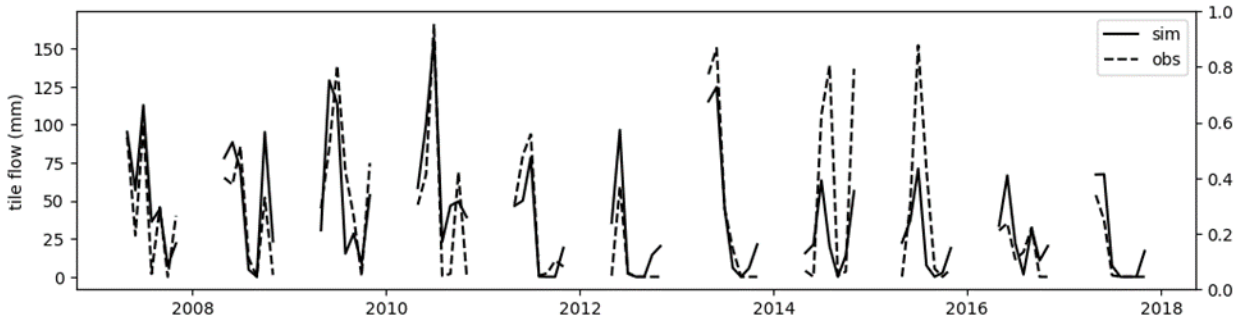

Figure S24. Monthly tile flow time series in the growing seasons./

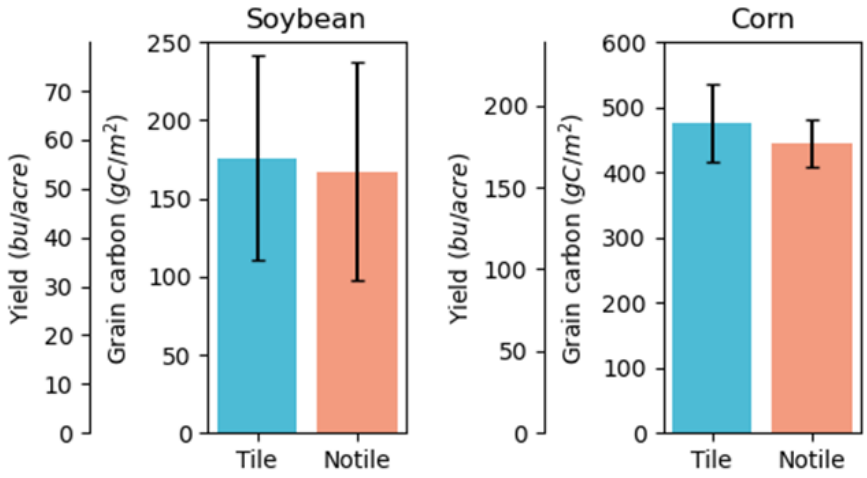

Figure S25. ***Ecosys*****-simulated multiyear mean crop yield (2007-2017).**

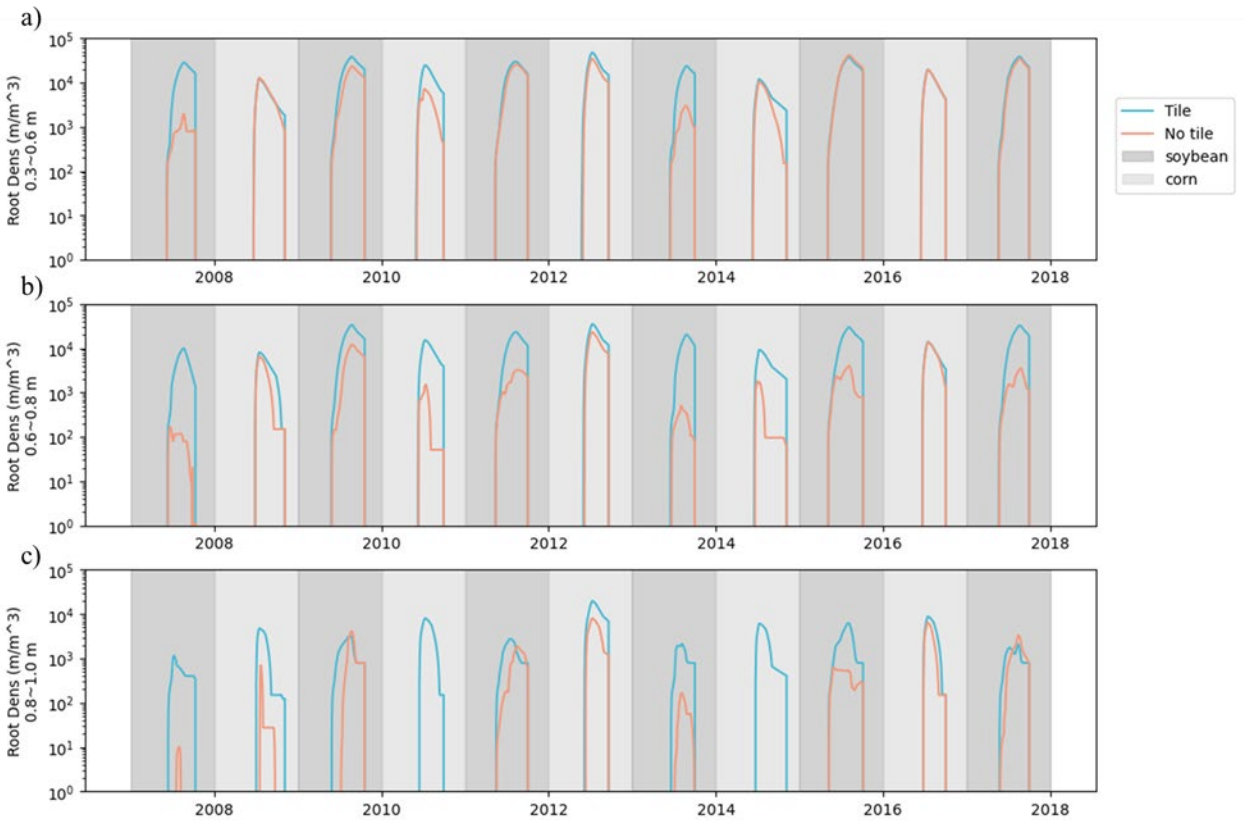

Figure S26. ***Ecosys*-simulated root density in three soil layers**: **a**) 0.3~0.6 m; **b**) 0.6~0.8 m; **c**) 0.8~1.0 m

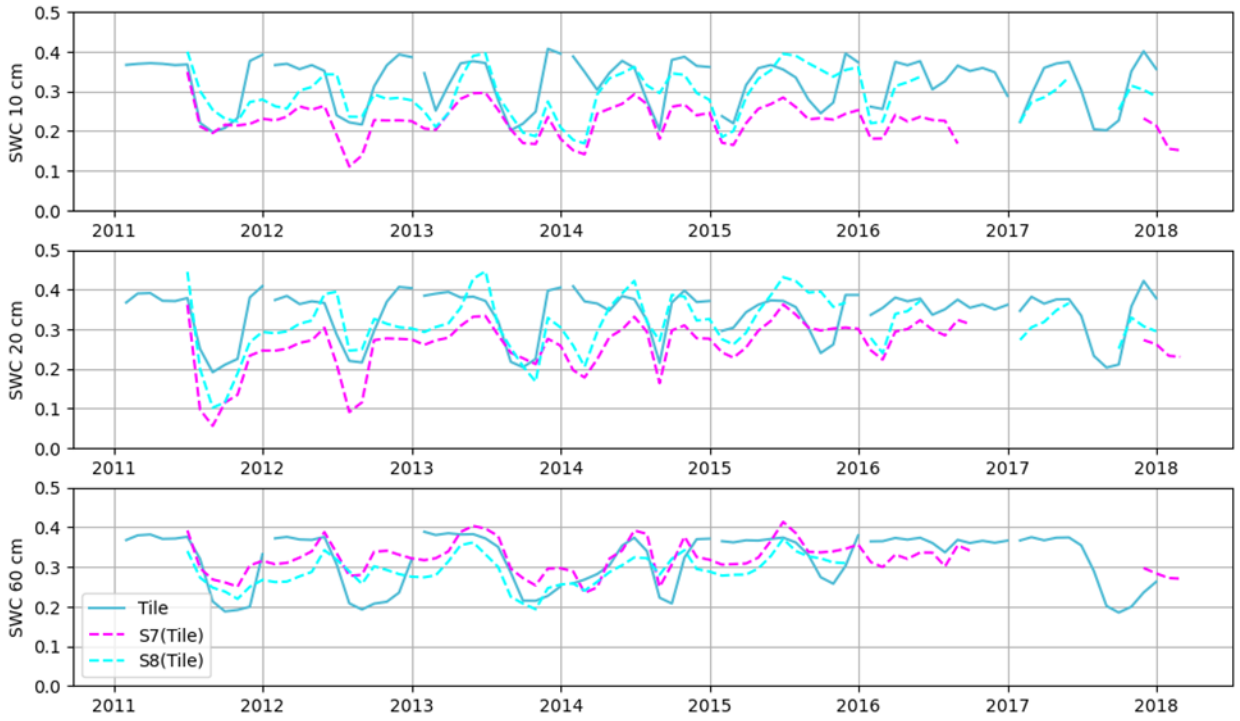

Figure S27. Validation for soil water content time series in tile field.

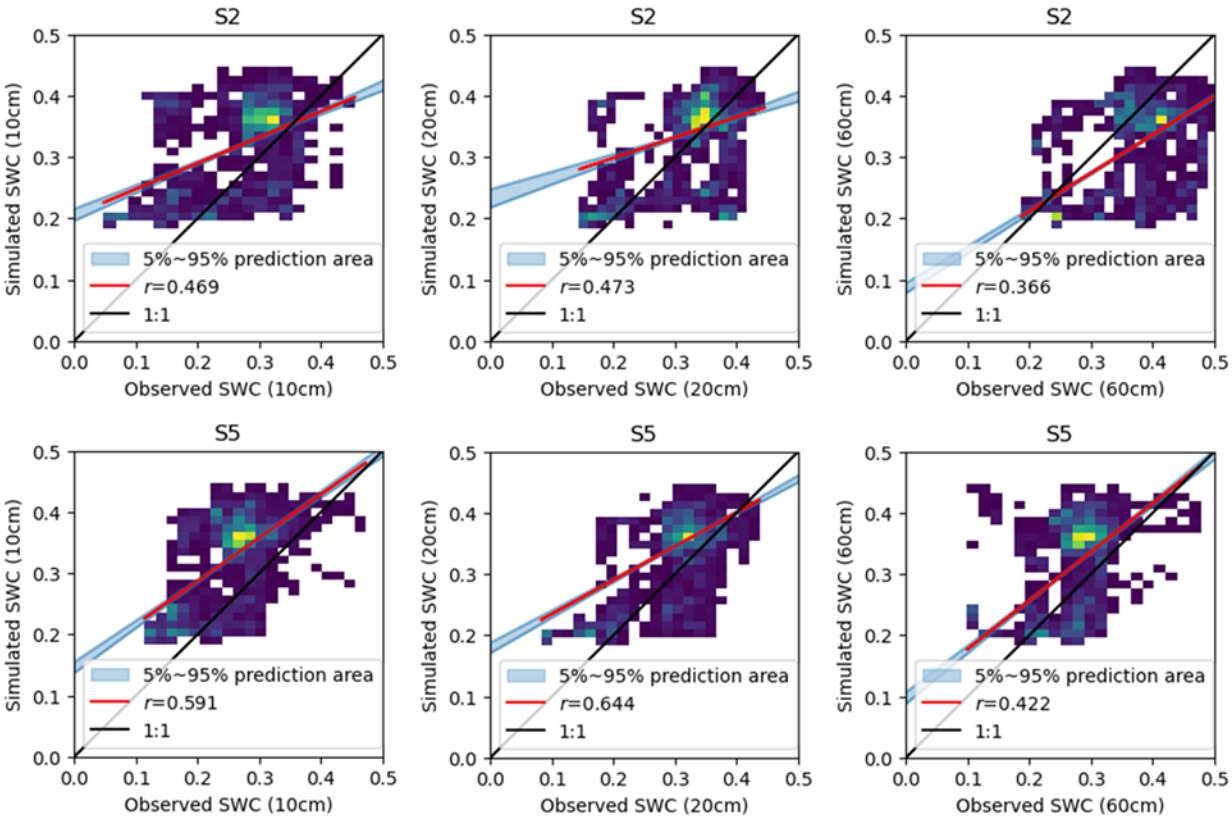

Figure S28. Validation for soil water content in tile field. S2 and S5 are two replicates of tile drainage sites.

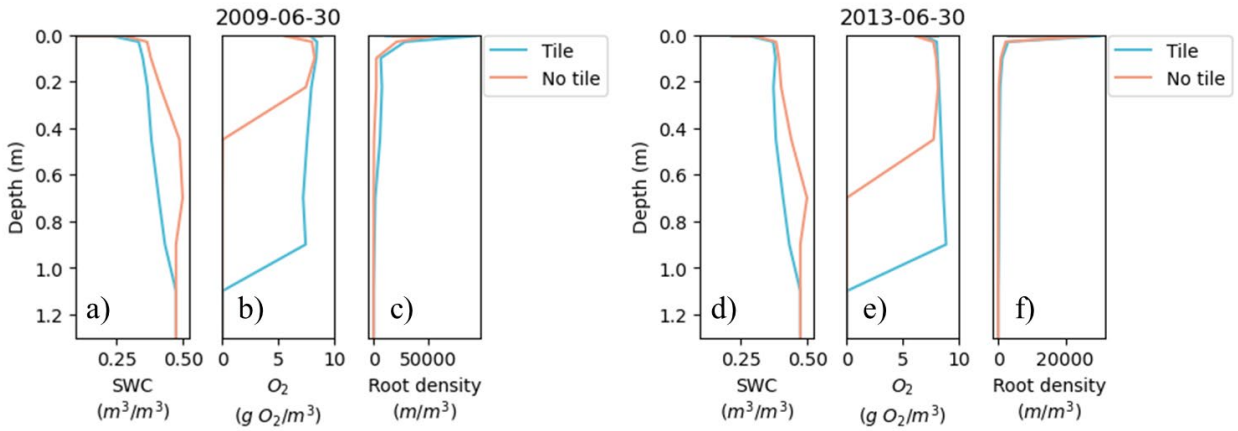

Figure S29. *Ecosys*-simulated soil profile. The profile of **a**) Soil water content, **b**) soil O_2 concentration, and **c**) root density profiles in the soil column on June 30th, 2009. The profile of **d**) Soil water content, **e**) soil O_2 concentration, and **f**) root density profiles in the soil column on June 30th, 2013. The x axis of c) and f) is in linear scale

Supplemented Tables

Table S1. Calibrated plant parameters in *ecosys*

	Parameters	Explanation
Corn	GroupX	Plant maturity group: Node number required to start floral initiation (-)
	Chl4	Fraction of leaf protein in mesophyll chlorophyll for C4 plants (-)
	Gfill	Maximum rate of kernel filling (g seed-1 h-1)
	RCS	Shape parameter for stomatal resistance vs leaf turgor potential (-)
	XKCO2	Rate constant for Rubisco Carboxylation (uM)
Soybean	GroupX	Plant maturity group: Node number required to start floral initiation (-)
	VCMX	Specific rubisco carboxylase activity (umol g-1 s-1)
	Gfill	Maximum rate of kernel filling (g seed-1 h-1)
	RCS	Shape parameter for stomatal resistance vs leaf turgor potential (-)
	XKCO2	Rate constant for Rubisco Carboxylation (uM)

Reference

Chighladze, G., Abendroth, L. J., Herzmann, D., Helmers, M., Ahiablame, L., Allred, B., Bowling, L., Brown, L., Fausey, N., Frankenberger, J., and Others: Transforming Drainage Research Data (USDA-NIFA Award No. 2015-68007-23193), National Agricultural Library--ARS--USDA, 2021.

Grant, R. F.: Simulation model of soil compaction and root growth, Plant Soil, 150, 1–14, 1993.

Grant, R. F.: Simulation in ecosys of root growth response to contrasting soil water and nitrogen, Ecol. Modell., 107, 237–264, 1998.

Grant, R. F. and Pattey, E.: Modelling variability in N2O emissions from fertilized agricultural fields, Soil Biol. Biochem., 35, 225–243, 2003.

Grant, R. F., Rochette, P., and Desjardins, R. L.: Energy exchange and water use efficiency of field crops: Validation of a simulation model, Agron. J., 85, 916–928, 1993a.

Grant, R. F., Nyborg, M., and Laidlaw, J. W.: Evolution of nitrous oxide from soil: I. Model development, Soil Sci., 156, 259, 1993b.

Grant, R. F., Juma, N. G., and McGill, W. B.: Simulation of carbon and nitrogen transformations in soil: Mineralization, Soil Biol. Biochem., 25, 1317–1329, 1993c.

Hodge, A., Berta, G., Doussan, C., Merchan, F., and Crespi, M.: Plant root growth, architecture and function, Plant Soil, 321, 153–187, 2009.

Jaynes, D. B., Hatfield, J. L., and Meek, D. W.: Water quality in Walnut Creek watershed: Herbicides and nitrate in surface waters, J. Environ. Qual., 28, 45–59, 1999.

Jin, W., Aufrecht, J., Patino-Ramirez, F., Cabral, H., Arson, C., and Retterer, S. T.: Modeling root system growth around obstacles, Sci. Rep., 10, 15868, 2020.

Lesk, C., Rowhani, P., and Ramankutty, N.: Influence of extreme weather disasters on global crop production, Nature, 529, 84–87, 2016.

Li, Y., Guan, K., Yu, A., Peng, B., Zhao, L., Li, B., and Peng, J.: Toward building a transparent statistical model for improving crop yield prediction: Modeling rainfed corn in the U.S, Field Crops Res., 234, 55–65, 2019.

Lobell, D. B., Roberts, M. J., Schlenker, W., Braun, N., Little, B. B., Rejesus, R. M., and Hammer, G. L.: Greater sensitivity to drought accompanies maize yield increase in the U.S. Midwest, Science, 344, 516–519, 2014.

NASS-USDA: 2017 Census of Agriculture, 2017.

Schmidhuber, J. and Tubiello, F. N.: Global food security under climate change, Proc. Natl. Acad. Sci. U. S. A., 104, 19703–19708, 2007.

Seneviratne, S. I., Adnan, M., Badi, W., Dereczynski, C., Luca, A. D., Ghosh, S., Iskandar, I., Kossin, J., Lewis, S., Otto, F., Pinto, I., Satoh, M., Vicente-Serrano, S. M., Wehner, M., and Zhou, B.: Weather and climate extreme events in a changing climate, Climate Change 2021: The Physical Science Basis. Contribution of Working Group I to the Sixth Assessment Report of the Intergovernmental Panel on Climate Change, 1513–1766, 2022.

Zhou, W., Ruby Leung, L., and Lu, J.: Seasonally Dependent Future Changes in the U.S. Midwest Hydroclimate and Extremes, J. Clim., 35, 17–27, 2022.